
Distral: Robust Multitask Reinforcement Learning

Yee Whye Teh, Victor Bapst, Wojciech Marian Czarnecki, John Quan,
James Kirkpatrick, Raia Hadsell, Nicolas Heess, Razvan Pascanu

DeepMind, London, UK

{ywteh,vbapst,lejlot,johnquan,kirkpatrick,raia,heess,razp}@google.com

Abstract

Most deep reinforcement learning algorithms are data inefficient in complex and rich environments, limiting their applicability to many scenarios. One direction for improving data efficiency is multitask learning with shared neural network parameters, where efficiency may be improved through transfer across related tasks. In practice, however, this is not usually observed, because gradients from different tasks can interfere negatively, making learning unstable and sometimes even less data efficient. Another issue is the different reward schemes between tasks, which can easily lead to one task dominating the learning of a shared model. We propose a new approach for joint training of multiple tasks, which we refer to as Distral (**Distill & transfer learning**). Instead of sharing parameters between the different workers, we propose to share a “distilled” policy that captures common behaviour across tasks. Each worker is trained to solve its own task while constrained to stay close to the shared policy, while the shared policy is trained by distillation to be the centroid of all task policies. Both aspects of the learning process are derived by optimizing a joint objective function. We show that our approach supports efficient transfer on complex 3D environments, outperforming several related methods. Moreover, the proposed learning process is more robust and more stable—attributes that are critical in deep reinforcement learning.

1 Introduction

Deep Reinforcement Learning is an emerging subfield of Reinforcement Learning (RL) that relies on deep neural networks as function approximators that can scale RL algorithms to complex and rich environments. One key work in this direction was the introduction of DQN [17] which is able to play many games in the ATARI suite of games [2] at above human performance. However the agent requires a fairly large amount of time and data to learn effective policies and the learning process itself can be quite unstable, even with innovations introduced to improve wall clock time, data efficiency, and robustness by changing the learning algorithm [23, 29] or by improving the optimizer [16, 25]. A different approach was introduced by [12, 15, 14], whereby data efficiency is improved by training additional auxiliary tasks jointly with the RL task.

With the success of deep RL has come interest in increasingly complex tasks and a shift in focus towards scenarios in which a single agent must solve multiple related problems, either simultaneously or sequentially. Due to the large computational cost, making progress in this direction requires robust algorithms which do not rely on task-specific algorithmic design or extensive hyperparameter tuning. Intuitively, solutions to related tasks should facilitate learning since the tasks share common structure, and thus one would expect that individual tasks should require less data or achieve a higher asymptotic performance. Indeed this intuition has long been pursued in the multitask and transfer-learning literature [3, 27, 30, 6].

Somewhat counter-intuitively, however, the above is often not the result encountered in practice, particularly in the RL domain [22, 19]. Instead, the multitask and transfer learning scenarios are

frequently found to pose additional challenges to existing methods. Instead of making learning easier it is often observed that training on multiple tasks can negatively affect performances on the individual tasks, and additional techniques have to be developed to counteract this [22, 19]. It is likely that gradients from other tasks behave as noise, interfering with learning, or, in another extreme, one of the tasks might dominate the others.

In this paper we develop an approach for multitask and transfer RL that allows effective sharing of behavioral structure across tasks, giving rise to several algorithmic instantiations. In addition to some instructive illustrations on a grid world domain, we provide a detailed analysis of the resulting algorithms via comparisons to A3C [16] baselines on a variety of tasks in a first-person, visually-rich, 3D environment (DeepMind Lab [1]). We find that the Distral algorithms learn faster and achieve better asymptotic performance, are significantly more robust to hyperparameter settings, and learn more stably than multitask A3C baselines.

2 Distral: Distill and Transfer Learning

We propose a framework for simultaneous reinforcement learning of multiple tasks which we call Distral. Figure 1 provides a high level illustration involving four tasks. The method is founded on the notion of a shared policy (shown in the centre) which distills (in the sense of Bucila and Hinton et al. [5, 11]) common behaviours or representations from task-specific policies [22, 19]. Crucially, the distilled policy is then used to guide task-specific policies via regularization using a Kullback-Leibler (KL) divergence. The effect is akin to a shaping reward which can, for instance, overcome random walk exploration bottlenecks. In this way, knowledge gained in one task is distilled into the shared policy, then transferred to other tasks.

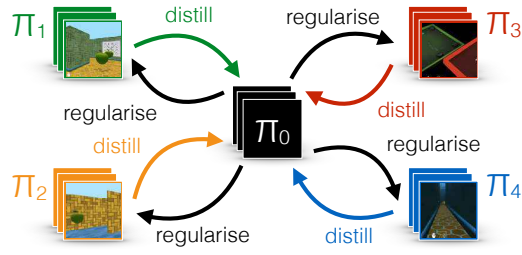


Figure 1: Illustration of the Distral framework.

2.1 Mathematical framework

In this section we describe the mathematical framework underlying Distral. A multitask RL setting is considered where there are n tasks, where for simplicity we assume an infinite horizon with discount factor γ .¹ We will assume that the action A and state S spaces are the same across tasks; we use $a \in A$ to denote actions, $s \in S$ to denote states. The transition dynamics $p_i(s'|s, a)$ and reward functions $R_i(a, s)$ are different for each task i . Let π_i be task-specific stochastic policies. The dynamics and policies give rise to joint distributions over state and action trajectories starting from some initial state, which we will also denote by π_i by an abuse of notation.

Our mechanism for linking the policy learning across tasks is via optimising an objective which consists of expected returns and policy regularizations. We designate π_0 to be the *distilled policy* which we believe will capture agent behaviour that is common across the tasks. We regularize each task policy π_i towards the distilled policy using γ -discounted KL divergences $\mathbb{E}_{\pi_i} [\sum_{t \geq 0} \gamma^t \log \frac{\pi_i(a_t|s_t)}{\pi_0(a_t|s_t)}]$. In addition, we also use a γ -discounted entropy regularization to further encourage exploration. The resulting objective to be maximized is:

$$\begin{aligned} J(\pi_0, \{\pi_i\}_{i=1}^n) &= \sum_i \mathbb{E}_{\pi_i} \left[\sum_{t \geq 0} \gamma^t R_i(a_t, s_t) - c_{\text{KL}} \gamma^t \log \frac{\pi_i(a_t|s_t)}{\pi_0(a_t|s_t)} - c_{\text{Ent}} \gamma^t \log \pi_i(a_t|s_t) \right] \\ &= \sum_i \mathbb{E}_{\pi_i} \left[\sum_{t \geq 0} \gamma^t R_i(a_t, s_t) + \frac{\gamma^t \alpha}{\beta} \log \pi_0(a_t|s_t) - \frac{\gamma^t}{\beta} \log \pi_i(a_t|s_t) \right] \end{aligned} \quad (1)$$

where $c_{\text{KL}}, c_{\text{Ent}} \geq 0$ are scalar factors which determine the strengths of the KL and entropy regularizations, and $\alpha = c_{\text{KL}}/(c_{\text{KL}} + c_{\text{Ent}})$ and $\beta = 1/(c_{\text{KL}} + c_{\text{Ent}})$. The $\log \pi_0(a_t|s_t)$ term can be thought

¹The method can be easily generalized to other scenarios like undiscounted finite horizon.

of as a reward shaping term which encourages actions which have high probability under the distilled policy, while the entropy term $-\log \pi_i(a_t|s_t)$ encourages exploration. In the above we used the same regularization costs $c_{\text{KL}}, c_{\text{Ent}}$ for all tasks. It is easy to generalize to using task-specific costs; this can be important if tasks differ substantially in their reward scales and amounts of exploration needed, although it does introduce additional hyperparameters that are expensive to optimize.

2.2 Soft Q-Learning and Distillation

A range of optimization techniques in the literature can be applied to maximize the above objective, which we will expand on below. To build up intuition for how the method operates, we will start in the simple case of a tabular representation and an alternating maximization procedure which optimizes over π_i given π_0 and over π_0 given π_i . With π_0 fixed, (1) decomposes into separate maximization problems for each task, and is an entropy regularized expected return with redefined (regularized) reward $R'_i(a, s) := R_i(a, s) + \frac{\alpha}{\beta} \log \pi_0(a|s)$. It can be optimized using soft Q-learning aka G learning, which are based on deriving the following “softened” Bellman updates for the state and action values (see [21, 8, 24, 18] for derivations):

$$V_i(s_t) = \frac{1}{\beta} \log \sum_{a_t} \pi_0^\alpha(a_t|s_t) \exp[\beta Q_i(a_t, s_t)] \quad (2)$$

$$Q_i(a_t, s_t) = R_i(a_t, s_t) + \gamma \sum_{s_{t+1}} p_i(s_{t+1}|s_t, a_t) V_i(s_{t+1}) \quad (3)$$

The Bellman updates are softened in the sense that the usual max operator over actions for the state values V_i is replaced by a soft-max at inverse temperature β , which hardens into a max operator as $\beta \rightarrow \infty$. The optimal policy π_i is then a Boltzmann policy at inverse temperature β :

$$\pi_i(a_t|s_t) = \pi_0^\alpha(a_t|s_t) e^{\beta Q_i(a_t|s_t) - \beta V_i(s_t)} = \pi_0^\alpha(a_t|s_t) e^{\beta A_i(a_t|s_t)} \quad (4)$$

where $A_i(a, s) = Q_i(a, s) - V_i(s)$ is a softened advantage function. Note that the softened state values $V_i(s)$ act as the log normalizers in the above. The distilled policy π_0 can be interpreted as a policy prior, a perspective well-known in the literature on RL as probabilistic inference [28, 13, 21, 8]. However, unlike in past works, it is raised to a power of $\alpha \leq 1$. This softens the effect of the prior π_0 on π_i , and is the result of the additional entropy regularization beyond the KL divergence.

Also unlike past works, we will learn π_0 instead of hand-picking it (typically as a uniform distribution over actions). In particular, notice that the only terms in (1) depending on π_0 are:

$$\frac{\alpha}{\beta} \sum_i \mathbb{E}_{\pi_i} \left[\sum_{t \geq 0} \gamma^t \log \pi_0(a_t|s_t) \right] \quad (5)$$

which is simply a log likelihood for fitting a model π_0 to a mixture of γ -discounted state-action distributions, one for each task i under policy π_i . A maximum likelihood (ML) estimator can be derived from state-action visitation frequencies under roll-outs in each task, with the optimal ML solution given by the mixture of state-conditional action distributions. Alternatively, in the non-tabular case, stochastic gradient ascent can be employed, which leads precisely to an update which distills the task policies π_i into π_0 [5, 11, 22, 19]. Note however that in our case the distillation step is derived naturally from a KL regularized objective on the policies. Another difference from [22, 19] and from prior works on the use of distillation in deep learning [5, 11] is that the distilled policy is “fed back in” to improve the task policies when they are next optimized, and serves as a conduit in which common and transferable knowledge is shared across the task policies.

It is worthwhile here to take pause and ponder the effect of the extra entropy regularization. First suppose that there is no extra entropy regularization, $\alpha = 1$, and consider the simple scenario of only $n = 1$ task. Then (5) is maximized when the distilled policy π_0 and the task policy π_1 are equal, and the KL regularization term is 0. Thus the objective reduces to an unregularized expected return, and so the task policy π_1 converges to a greedy policy which locally maximizes expected returns. Another way to view this line of reasoning is that the alternating maximization scheme is equivalent to trust-region methods like natural gradient or TRPO [20, 25] which use a KL ball centred at the previous policy, and which are understood to converge to greedy policies.

If $\alpha < 1$, there is an additional entropy term in (1). So even with $\pi_0 = \pi_1$ and $\text{KL}(\pi_1||\pi_0) = 0$, the objective (1) will no longer be maximized by greedy policies. Instead (1) reduces to an entropy

regularized expected returns with entropy regularization factor $\beta' = \beta/(1 - \alpha) = 1/c_{\text{Ent}}$, so that the optimal policy is of the Boltzmann form with inverse temperature β' [21, 8, 24, 18]. In conclusion, by including the extra entropy term, we can guarantee that the task policy will not turn greedy, and we can control the amount of exploration by adjusting c_{Ent} appropriately.

This additional control over the amount of exploration is essential when there are more than one task. To see this, imagine a scenario where one of the tasks is easier and is solved first, while other tasks are harder with much sparser rewards. Without the entropy term, and before rewards in other tasks are encountered, both the distilled policy and all the task policies can converge to the one that solves the easy task. Further, because this policy is greedy, it can insufficiently explore the other tasks to even encounter rewards, leading to sub-optimal behaviour. For single-task RL, the use of entropy regularization was recently popularized by Mnih et al. [16] to counter premature convergence to greedy policies, which can be particularly severe when doing policy gradient learning. This carries over to our multitask scenario as well, and is the reason for the additional entropy regularization.

2.3 Policy Gradient and a Better Parameterization

The above method alternates between maximization of the distilled policy π_0 and the task policies π_i , and is reminiscent of the EM algorithm [7] for learning latent variable models, with π_0 playing the role of parameters, while π_i plays the role of the posterior distributions for the latent variables. Going beyond the tabular case, when both π_0 and π_i are parameterized by, say, deep networks, such an alternating maximization procedure can be slower than simply optimizing (1) with respect to task and distilled policies jointly by stochastic gradient ascent. In this case the gradient update for π_i is simply given by policy gradient with an entropic regularization [16, 24], and can be carried out within a framework like advantage actor-critic [16].

A simple parameterization of policies would be to use a separate network for each task policy π_i , and another one for the distilled policy π_0 . An alternative parameterization, which we argue can result in faster transfer, can be obtained by considering the form of the optimal Boltzmann policy (4). Specifically, consider parameterizing the distilled policy using a network with parameters θ_0 ,

$$\hat{\pi}_0(a_t|s_t) = \frac{\exp(h_{\theta_0}(a_t|s_t))}{\sum_{a'} \exp(h_{\theta_0}(a'|s_t))} \quad (6)$$

and estimating the soft advantages² using another network with parameters θ_i :

$$\hat{A}_i(a_t|s_t) = f_{\theta_i}(a_t|s_t) - \frac{1}{\beta} \log \sum_a \hat{\pi}_0^\alpha(a|s_t) \exp(\beta f_{\theta_i}(a|s_t)) \quad (7)$$

We used hat notation to denote parameterized approximators of the corresponding quantities. The policy for task i then becomes parameterized as,

$$\hat{\pi}_i(a_t|s_t) = \hat{\pi}_0^\alpha(a_t|s_t) \exp(\beta \hat{A}_i(a_t|s_t)) = \frac{\exp(\alpha h_{\theta_0}(a_t|s_t) + \beta f_{\theta_i}(a_t|s_t))}{\sum_{a'} \exp((\alpha h_{\theta_0}(a'|s_t) + \beta f_{\theta_i}(a'|s_t))} \quad (8)$$

This can be seen as a two-column architecture for the policy, with one column being the distilled policy, and the other being the adjustment required to specialize to task i .

Given the parameterization above, we can now derive the policy gradients. The gradient wrt to the task specific parameters θ_i is given by the standard policy gradient theorem [26],

$$\begin{aligned} \nabla_{\theta_i} J &= \mathbb{E}_{\hat{\pi}_i} \left[\left(\sum_{t \geq 1} \nabla_{\theta_i} \log \hat{\pi}_i(a_t|s_t) \right) \left(\sum_{u \geq 1} \gamma^u (R_i^{\text{reg}}(a_u, s_u)) \right) \right] \\ &= \mathbb{E}_{\hat{\pi}_i} \left[\sum_{t \geq 1} \nabla_{\theta_i} \log \hat{\pi}_i(a_t|s_t) \left(\sum_{u \geq t} \gamma^u (R_i^{\text{reg}}(a_u, s_u)) \right) \right] \end{aligned} \quad (9)$$

where $R_i^{\text{reg}}(a, s) = R_i(a, s) + \frac{\alpha}{\beta} \log \hat{\pi}_0(a|s) - \frac{1}{\beta} \log \hat{\pi}_i(a|s)$ is the regularized reward. Note that the partial derivative of the entropy in the integrand has expectation $\mathbb{E}_{\hat{\pi}_i} [\nabla_{\theta_i} \log \hat{\pi}_i(a_t|s_t)] = 0$ because of the log-derivative trick. If a value baseline is estimated, it can be subtracted from the regularized

²In practice, we do not actually use these as advantage estimates. Instead we use (8) to parameterize a policy which is optimized by policy gradients.

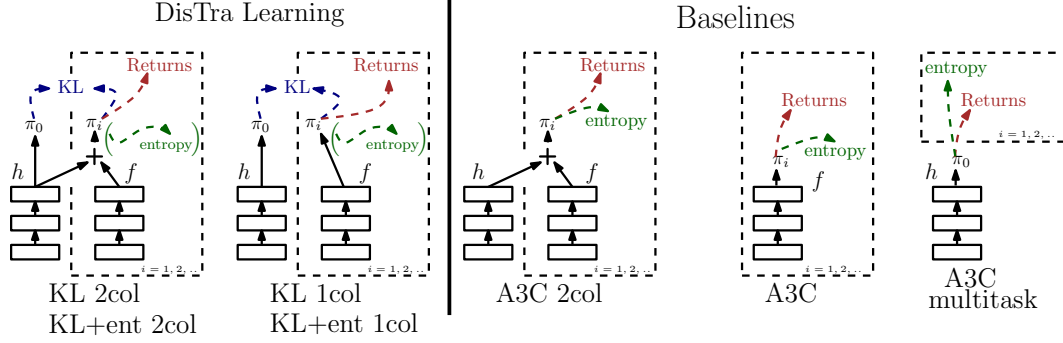


Figure 2: Depiction of the different algorithms and baselines. On the left are two of the Distral algorithms and on the right are the three A3C baselines. Entropy is drawn in brackets as it is optional and only used for KL+ent 2col and KL+ent 1col.

returns in order to reduce gradient variance. The gradient wrt θ_0 is more interesting:

$$\begin{aligned} \nabla_{\theta_0} J = & \sum_i \mathbb{E}_{\hat{\pi}_i} \left[\sum_{t \geq 1} \nabla_{\theta_0} \log \hat{\pi}_i(a_t | s_t) \left(\sum_{u \geq t} \gamma^u R_i^{\text{reg}}(a_u, s_u) \right) \right] \\ & + \frac{\alpha}{\beta} \sum_i \mathbb{E}_{\hat{\pi}_i} \left[\sum_{t \geq 1} \gamma^t \sum_{a'_t} (\hat{\pi}_i(a'_t | s_t) - \hat{\pi}_0(a'_t | s_t)) \nabla_{\theta_0} h_{\theta_0}(a'_t | s_t) \right] \end{aligned} \quad (10)$$

Note that the first term is the same as for the policy gradient of θ_i . The second term tries to match the probabilities under the task policy $\hat{\pi}_i$ and under the distilled policy $\hat{\pi}_0$. The second term would not be present if we simply parameterized π_i using the same architecture $\hat{\pi}_i$, but do not use a KL regularization for the policy. The presence of the KL regularization gets the distilled policy to learn to be the centroid of all task policies, in the sense that the second term would be zero if $\hat{\pi}_0(a'_t | s_t) = \frac{1}{n} \sum_i \hat{\pi}_i(a'_t | s_t)$, and helps to transfer information quickly across tasks and to new tasks.

The centroid and star-shaped structure of DisTraL is reminiscent of ADMM [4], elastic-averaging SGD [31] and hierarchical Bayes [10]. Though a crucial difference is that while ADMM, EASGD and hierarchical Bayes operate in the space of parameters, in Distral the distilled policy learns to be the centroid in the space of policies. We argue that this is semantically more meaningful, and may contribute to the observed robustness of Distral by stabilizing learning. In our experiments we find indeed that absence of the KL regularization significantly affects the stability of the algorithm.

Our approach is also reminiscent of recent work on option learning [9], but with a few important differences. We focus on using deep neural networks as flexible function approximators, and applied our method to rich 3D visual environments, while Fox et al. [9] considered only the tabular case. We argue for the importance of an additional entropy regularization besides the KL regularization. This lead to an interesting twist in the mathematical framework allowing us to separately control the amounts of transfer and of exploration. On the other hand Fox et al. [9] focused on the interesting problem of learning multiple options (distilled policies here). Their approach treats the assignment of tasks to options as a clustering problem, which is not easily extended beyond the tabular case.

3 Algorithms

The framework we just described allows for a number of possible algorithmic instantiations, arising as combinations of objectives, algorithms and architectures, which we describe below and summarize in Table 1 and Figure 2. *KL divergence vs entropy regularization*: With $\alpha = 0$, we get a purely entropy-regularized objective which does not couple and transfer across tasks [16, 24]. With $\alpha = 1$, we get a purely KL regularized objective, which does couple and transfer across tasks, but might prematurely stop exploration if the distilled and task policies become similar and greedy. With $0 < \alpha < 1$ we get both terms. *Alternating vs joint optimization*: We have the option of jointly optimizing both the distilled policy and the task policies, or optimizing one while keeping the other fixed. Alternating optimization leads to algorithms that resemble policy distillation/actor-mimic [19, 22], but are iterative in nature with the distilled policy feeding back into task policy optimization. Also, soft Q-learning can be applied to each task, instead of policy gradients. While alternating

	$h_{\theta_0}(a s)$	$f_{\theta_i}(a s)$	$\alpha h_{\theta_0}(a s) + \beta f_{\theta_i}(a s)$
$\alpha = 0$	A3C multitask	A3C	A3C 2col
$\alpha = 1$		KL 1col	KL 2col
$0 < \alpha < 1$		KL+ent 1col	KL+ent 2col

Table 1: The seven different algorithms evaluated in our experiments. Each column describes a different architecture, with the column headings indicating the logits for the task policies. The rows define the relative amount of KL vs entropy regularization loss, with the first row comprising the A3C baselines (no KL loss).

optimization can be slower, evidence from policy distillation/actor-mimic indicate it might learn more stably, particularly for tasks which differ significantly. *Separate vs two-column parameterization*: Finally, the task policy can be parameterized to use the distilled policy (8) or not. If using the distilled policy, behaviour distilled into the distilled policy is “immediately available” to the task policies so transfer can be faster. However if the process of transfer occurs too quickly, it might prevent effective exploration of individual tasks.

From this spectrum of possibilities we consider four concrete instances which differ in the underlying network architecture and distillation loss, identified in Table 1. In addition, we compare against three A3C baselines. In initial experiments we explored two variants of A3C: the original method [16] and the variant of Schulman et al. [24] which uses entropy regularized returns. We did not find significant differences for the two variants in our setting, and chose to report only the original A3C results for clarity in Section 4. Further algorithmic details are provided in the Appendix.

4 Experiments

We demonstrate the various algorithms derived from our framework, firstly using alternating optimization with soft Q-learning and policy distillation on a set of simple grid world tasks. Then all seven algorithms will be evaluated on three sets of challenging RL tasks in partially observable 3D environments [1].

4.1 Two room grid world

To give better intuition for the role of the distilled behaviour policy, we considered a set of tasks in a grid world domain with two rooms connected by a corridor (see Figure 3) [9]. Each task is distinguished by a different randomly chosen goal location and each MDP state consists of the map location, the previous action and the previous reward. A Distral agent is trained using only the KL regularization and an optimization algorithm which alternates between soft Q-learning and policy distillation. Each soft Q-learning iteration learns using a rollout of length 10.

To determine the benefit of the distilled policy, we compared the Distral agent to one which soft Q learns a separate policy for each task. The learning curves are shown in Figure 3 (left). We see that the Distral agent is able to learn significantly faster than single-task agents. Figure 3 (right) visualizes the distilled policy (probability of next action given position and previous action), demonstrating that the agent has learnt a robust policy which guides the agent to move consistently in the corridor in order to reach the other room. This allows the agent to reach the other room faster and helps exploration, if the agent is shown new test tasks. In Fox et al. [9] two separate options are learnt, while here we learn a single distilled policy which conditions on more past information.

4.2 Complex Tasks

To assess Distral under more challenging conditions, we use a complex first-person partially observed 3D environment with a variety of visually-rich RL tasks [1]. All agents were implemented with a distributed Python/TensorFlow code base, using 32 workers for each task and learnt using asynchronous RMSProp. The network columns contain convolutional layers and an LSTM and are uniform across experiments and algorithms. We tried three values for the entropy costs β and three learning rates ϵ . Four runs for each hyperparameter setting were used. All other hyperparameters were fixed to the

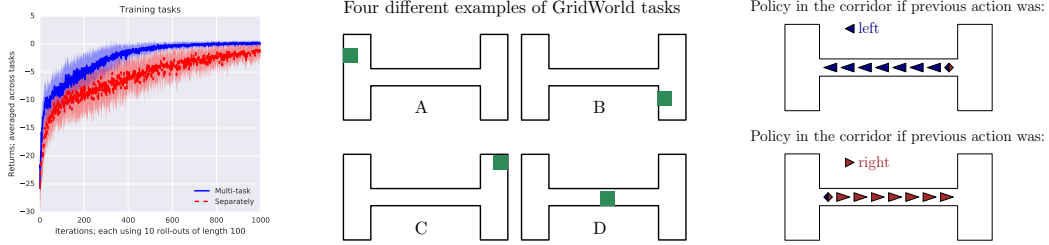


Figure 3: **Left:** Learning curves on two room grid world. The DisTraL agent (blue) learns faster, converges towards better policies, and demonstrates more stable learning overall. **Center:** Example of tasks. Green is goal position which is uniformly sampled for each task. Starting position is uniformly sampled at the beginning of each episode. **Right:** depiction of learned distilled policy π_0 only in the corridor, conditioned on previous action being left/right and no previous reward. Sizes of arrows depict probabilities of actions. Note that up/down actions have negligible probabilities. The model learns to preserve direction of travel in the corridor.

single-task A3C defaults and, for the KL+ent_1col and KL+ent_2col algorithms, α was fixed at 0.5.

Mazes In the first experiment, each of $n = 8$ tasks is a different maze containing randomly placed rewards and a goal object. Figure 4.A1 shows the learning curves for all seven algorithms. Each curve is produced by averaging over all 4 runs and 8 tasks, and selecting the best settings for β and ϵ (as measured by the area under the learning curves). The Distral algorithms learn faster and achieve better final performance than all three A3C baselines. The two-column algorithms learn faster than the corresponding single column ones. The Distral algorithms without entropy learn faster but achieve lower final scores than those with entropy, which we believe is due to insufficient exploration towards the end of learning.

We found that both multitask A3C and two-column A3C can learn well on some runs, but are generally unstable—some runs did not learn well, while others may learn initially then suffer degradation later. We believe this is due to negative interference across tasks, which does not happen for Distral algorithms. The stability of Distral algorithms also increases their robustness to hyperparameter selection. Figure 4.A2 shows the final achieved average returns for all 36 runs for each algorithm, sorted in decreasing order. We see that Distral algorithms have a significantly higher proportion of runs achieving good returns, with KL+ent_2col being the most robust.

DisTraL algorithms, along with multitask A3C, use a distilled or common policy which can be applied on all tasks. Panels B1 and B2 in Figure 4 summarize the performances of the distilled policies. Algorithms that use two columns (KL_2col and KL+ent_2col) obtain the best performance, because policy gradients are also directly propagated through the distilled policy in those cases. Moreover, panel B2 reveals that Distral algorithms exhibit greater stability as compared to traditional multitask A3C. We also observe that KL algorithms have better-performing distilled policies than KL+ent ones. We believe this is because the additional entropy regularization allows task policies to diverge more substantially from the distilled policy. This suggests that annealing the entropy term or increasing the KL term throughout training could improve the distilled policy performance, if that is of interest.

Navigation We experimented with $n = 4$ navigation and memory tasks. In contrast to the previous experiment, these tasks use random maps which are procedurally generated on every episode. The first task features reward objects which are randomly placed in a maze, and the second task requires to return these objects to the agent’s start position. The third task has a single goal object which must be repeatedly found from different start positions, and on the fourth task doors are randomly opened and closed to force novel path-finding. Hence, these tasks are more involved than the previous navigation tasks. The panels C1 and C2 of Figure 4 summarize the results. We observe again that Distral algorithms yield better final results while having greater stability (Figure 4.C2). The top-performing algorithms are, again, the 2 column Distral algorithms (KL_2col and KL+ent_2col).

Laser-tag In the final set of experiments, we use $n = 8$ laser-tag levels from DeepMind Lab. These tasks require the agent to learn to tag bots controlled by a built-in AI, and differ substantially: fixed versus procedurally generated maps, fixed versus procedural bots, and complexity of agent behaviour

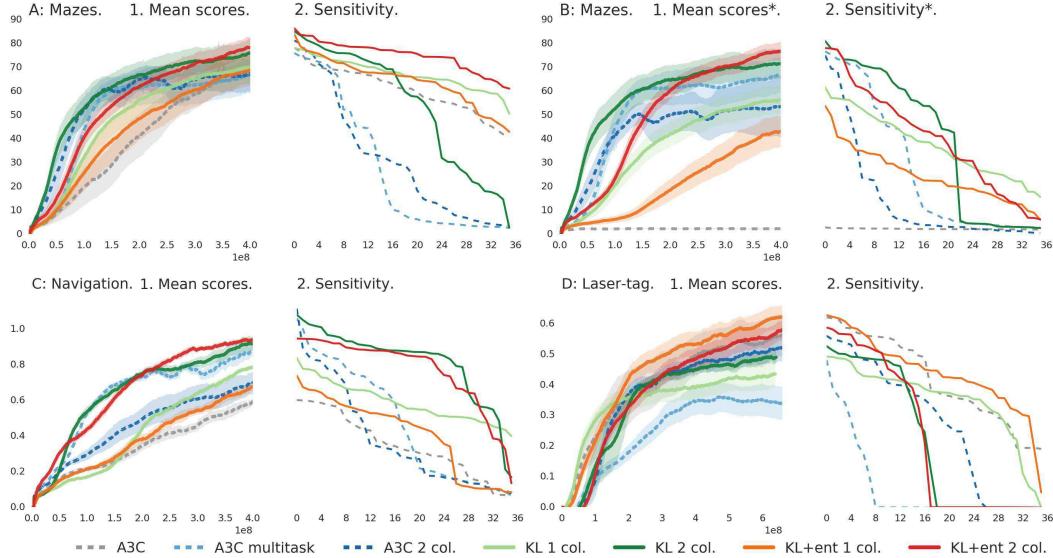


Figure 4: Panels A1, C1, D1 show task specific policy performance (averaged across all the tasks) for the maze, navigation and laser-tag tasks, respectively. The x -axes are total numbers of training environment steps per task. Panel B1 shows the mean scores obtained with the distilled policies (A3C has no distilled policy, so it is represented by the performance of an untrained network.). For each algorithm, results for the best set of hyperparameters (based on the area under curve) are reported. The bold line is the average over 4 runs, and the colored area the average standard deviation over the tasks. Panels A2, B2, C2, D2 shows the corresponding final performances for the 36 runs of each algorithm ordered by best to worst (9 hyperparameter settings and 4 runs).

(e.g. learning to jump in some tasks). Corresponding to this greater diversity, we observe (see panels D1 and D2 of Figure 4) that the best baseline is the A3C algorithm that is trained independently on each task. Among the Distral algorithms, the single column variants perform better, especially initially, as they are able to learn task-specific features separately. We observe again the early plateauing phenomenon for algorithms that do not possess an additional entropy term. While not significantly better than the A3C baseline on these tasks, the Distral algorithms clearly outperform the multitask A3C. Considering the 3 different sets of complex 3D experiments, we argue that the Distral algorithms are the most promising solution to the multitask RL problem.

5 Discussion

We have proposed Distral, a general framework for distilling and transferring common behaviours in multitask reinforcement learning. In experiments we showed that the resulting algorithms learn quicker, produce better final performances, and are more stable and robust to hyperparameter settings. We have found that Distral significantly outperforms the standard way of using shared neural network parameters for multitask or transfer reinforcement learning. Two ideas might be worth reemphasizing here. We observe that distillation arises naturally as one half of an optimization procedure when using KL divergences to regularize the output of task models towards a distilled model. The other half corresponds to using the distilled model as a regularizer for training the task models. Another observation is that parameters in deep networks do not typically by themselves have any semantic meaning, so instead of regularizing networks in parameter space, it is worthwhile considering regularizing networks in a more semantically meaningful space, e.g. of policies.

Possible directions of future research include: combining Distral with techniques which use auxiliary losses [12, 15, 14], exploring use of multiple distilled policies or latent variables in the distilled policy to allow for more diversity of behaviours, exploring settings for continual learning where tasks are encountered sequentially, and exploring ways to adaptively adjust the KL and entropy costs to better control the amounts of transfer and exploration.

References

- [1] Charles Beattie, Joel Z Leibo, Denis Teplyashin, Tom Ward, Marcus Wainwright, Heinrich Küttler, Andrew Lefrancq, Simon Green, Víctor Valdés, Amir Sadik, et al. Deepmind lab. *arXiv:1612.03801*, 2016.
- [2] M. G. Bellemare, Y. Naddaf, J. Veness, and M. Bowling. The arcade learning environment: An evaluation platform for general agents. *Journal of Artificial Intelligence Research*, 47:253–279, june 2013.
- [3] Yoshua Bengio. Deep learning of representations for unsupervised and transfer learning. In *JMLR: Workshop on Unsupervised and Transfer Learning*, 2012.
- [4] Stephen Boyd, Neal Parikh, Eric Chu, Borja Peleato, and Jonathan Eckstein. Distributed optimization and statistical learning via the alternating direction method of multipliers. *Found. Trends Mach. Learn.*, 3(1), January 2011.
- [5] Cristian Bucila, Rich Caruana, and Alexandru Niculescu-Mizil. Model compression. In *Proc. of the Int’l Conference on Knowledge Discovery and Data Mining (KDD)*, 2006.
- [6] Rich Caruana. Multitask learning. *Machine Learning*, 28(1):41–75, July 1997.
- [7] Arthur P Dempster, Nan M Laird, and Donald B Rubin. Maximum likelihood from incomplete data via the em algorithm. *Journal of the royal statistical society. Series B (methodological)*, pages 1–38, 1977.
- [8] R. Fox, A. Pakman, and N. Tishby. Taming the noise in reinforcement learning via soft updates. In *Uncertainty in Artificial Intelligence (UAI)*, 2016.
- [9] Roy Fox, Michal Moshkovitz, and Naftali Tishby. Principled option learning in markov decision processes. In *European Workshop on Reinforcement Learning (EWRL)*, 2016.
- [10] Andrew Gelman, John B Carlin, Hal S Stern, and Donald B Rubin. *Bayesian data analysis*, volume 2. Chapman & Hall/CRC Boca Raton, FL, USA, 2014.
- [11] Geoffrey E. Hinton, Oriol Vinyals, and Jeffrey Dean. Distilling the knowledge in a neural network. *NIPS Deep Learning Workshop*, 2014.
- [12] Max Jaderberg, Volodymyr Mnih, Wojciech Marian Czarnecki, Tom Schaul, Joel Z Leibo, David Silver, and Koray Kavukcuoglu. Reinforcement learning with unsupervised auxiliary tasks. *Int’l Conference on Learning Representations (ICLR)*, 2016.
- [13] Hilbert J Kappen, Vicenç Gómez, and Manfred Opper. Optimal control as a graphical model inference problem. *Machine learning*, 87(2):159–182, 2012.
- [14] Guillaume Lample and Devendra Singh Chaplot. Playing FPS games with deep reinforcement learning. *Association for the Advancement of Artificial Intelligence (AAAI)*, 2017.
- [15] Piotr Mirowski, Razvan Pascanu, Fabio Viola, Hubert Soyer, Andrew J. Ballard, Andrea Banino, Misha Denil, Ross Goroshin, Laurent Sifre, Koray Kavukcuoglu, Dharshan Kumaran, and Raia Hadsell. Learning to navigate in complex environments. *Int’l Conference on Learning Representations (ICLR)*, 2016.
- [16] Volodymyr Mnih, Adria Puigdomenech Badia, Mehdi Mirza, Alex Graves, Timothy P Lillicrap, Tim Harley, David Silver, and Koray Kavukcuoglu. Asynchronous methods for deep reinforcement learning. In *Int’l Conference on Machine Learning (ICML)*, 2016.
- [17] Volodymyr Mnih, Koray Kavukcuoglu, David Silver, Andrei A. Rusu, Joel Veness, Marc G. Bellemare, Alex Graves, Martin Riedmiller, Andreas K. Fiedland, Georg Ostrovski, Stig Petersen, Charles Beattie, Amir Sadik, Ioannis Antonoglou, Helen King, Dharshan Kumaran, Daan Wierstra, Shane Legg, and Demis Hassabis. Human-level control through deep reinforcement learning. *Nature*, 518(7540):529–533, 02 2015.
- [18] Ofir Nachum, Mohammad Norouzi, Kelvin Xu, and Dale Schuurmans. Bridging the gap between value and policy based reinforcement learning. *arXiv:1702.08892*, 2017.
- [19] Emilio Parisotto, Jimmy Lei Ba, and Ruslan Salakhutdinov. Actor-mimic: Deep multitask and transfer reinforcement learning. In *Int’l Conference on Learning Representations (ICLR)*, 2016.
- [20] Razvan Pascanu and Yoshua Bengio. Revisiting natural gradient for deep networks. *Int’l Conference on Learning Representations (ICLR)*, 2014.
- [21] Konrad Rawlik, Marc Toussaint, and Sethu Vijayakumar. On stochastic optimal control and reinforcement learning by approximate inference. In *Robotics: Science and Systems (RSS)*, 2012.
- [22] Andrei A Rusu, Sergio Gomez Colmenarejo, Caglar Gulcehre, Guillaume Desjardins, James Kirkpatrick, Razvan Pascanu, Volodymyr Mnih, Koray Kavukcuoglu, and Raia Hadsell. Policy distillation. In *Int’l Conference on Learning Representations (ICLR)*, 2016.

- [23] Tom Schaul, John Quan, Ioannis Antonoglou, and David Silver. Prioritized experience replay. *CoRR*, abs/1511.05952, 2015.
- [24] J. Schulman, P. Abbeel, and X. Chen. Equivalence between policy gradients and soft Q-Learning. *arXiv:1704.06440*, 2017.
- [25] John Schulman, Sergey Levine, Pieter Abbeel, Michael Jordan, and Philipp Moritz. Trust region policy optimization. In *Int’l Conference on Machine Learning (ICML)*, 2015.
- [26] Richard S Sutton, David A McAllester, Satinder P Singh, Yishay Mansour, et al. Policy gradient methods for reinforcement learning with function approximation. In *Adv. in Neural Information Processing Systems (NIPS)*, volume 99, pages 1057–1063, 1999.
- [27] Matthew E. Taylor and Peter Stone. An introduction to inter-task transfer for reinforcement learning. *AI Magazine*, 32(1):15–34, 2011.
- [28] Marc Toussaint, Stefan Harmeling, and Amos Storkey. Probabilistic inference for solving (PO)MDPs. Technical Report EDI-INF-RR-0934, University of Edinburgh, School of Informatics, 2006.
- [29] Hado van Hasselt, Arthur Guez, and David Silver. Deep reinforcement learning with double Q-learning. *Association for the Advancement of Artificial Intelligence (AAAI)*, 2016.
- [30] Jason Yosinski, Jeff Clune, Yoshua Bengio, and Hod Lipson. How transferable are features in deep neural networks? In *Adv. in Neural Information Processing Systems (NIPS)*, 2014.
- [31] Sixin Zhang, Anna Choromanska, and Yann LeCun. Deep learning with elastic averaging SGD. In *Adv. in Neural Information Processing Systems (NIPS)*, 2015.

	Num tasks	Inter-task variability	Map/maze layout	Objectives and Agent Behaviours
Mazes	8	low	Fixed layout for each task.	Collect a goal object multiple times from different start positions in the maze.
Navigation	4	medium	Procedurally varied on every episode.	Various objectives requiring memory and exploration skills, including collecting objects and navigating back to start location, and finding a goal object from multiple start positions with doors that randomly open and close.
Laser-tag	8	high	Fixed for some tasks and procedurally varied for others.	Tag bots controlled by the OpenArena AI while collecting objects to increase score. May require jumping and other agent behaviours.

Table 2: Details on the various tasks used in Section 4.2.

A Algorithms

A description of all the algorithms tested:

- **A3C**: A policy is trained separately for each task using A3C.
- **A3C_multitask**: A single policy is trained using A3C by simultaneously training on all tasks.
- **A3C_2col**: A policy is trained for each task using A3C, which is parameterized using a two-column architecture with one column shared across tasks (8).
- **KL_1col**: Each policy including the distilled policy is parameterized by one network, and trained to optimize (1) with $\alpha = 1$, i.e. only using the KL regularization.
- **KL+ent_1col**: Same as KL_1col but using both KL and entropy regularization. We set $\alpha = 0.5$ and did not tune for it in our experiments.
- **KL_2col**: Same as KL_1col but using the two-column architecture (8) with one shared network column which also produces the distilled policy $\hat{\pi}_0$.
- **KL+ent_2col**: Same as KL+ent_1col but using the two-column architecture.

B Experimental details

B.1 Two room grid world

The agent can stay put or move in each of the four cardinal coordinates. A penalty of -0.1 is incurred for every time step and a penalty of -0.5 is incurred if the agent runs into the wall. On reaching the goal state the episode terminates and the agent gets a reward of $+1$. We used learning rate of 0.1 , discount of 0.95 for soft Q-learning, $\beta = 5$, and regularized the distilled policy by using a pseudocount of 1 for each action in each state. The reported results are not sensitive to these settings and we did not tune for them.

B.2 Complex 3D tasks

The three sets of tasks are described in Table 2.

We implemented the updates (9-10) by training a distributed agent *a la* A3C [16] with 32 workers for each task, coordinated using parameter servers. The agent receives a RGB observation from the environment in the form of a $3 \times 84 \times 84$ tensor. Each network column has the same architecture as in Mnih et al. [16] and consists of two convolutional layers with ReLU nonlinearities, followed by a fully connected layer with 256 hidden units and ReLU nonlinearity, which then feeds into an LSTM. Policy logits and values are then read out linearly from the LSTM. We used RMSProp as an optimizer, and batches of length 20.

We used a set of 9 hyperparameters $(1/\beta, \epsilon) \in \{3 \cdot 10^{-4}, 10^{-3}, 3 \cdot 10^{-3}\} \times \{2 \cdot 10^{-4}, 4 \cdot 10^{-4}, 8 \cdot 10^{-4}\}$ for the entropy costs and initial learning rate. We kept $\alpha = 0.5$ throughout all runs of KL+ent_1col and KL+ent_2col (and, by definition, we have $\alpha = 0$ for A3C, A3C_multitask, A3C_2col and $\alpha = 1$ for KL_1col and KL_2col.). The learning rate was annealed linearly from its initial value ϵ down to $\epsilon/6$ over a total of N environment steps per task, where $N = 4 \cdot 10^8$ for the maze and navigation tasks, and $N = 6.6 \cdot 10^8$ for the laser-tag tasks. We used an action-repeat of 4 (each action output by the network is fed 4 times to the environment), so the number

of training steps in each environment is respectively 10^8 and $1.65 \cdot 10^8$. In addition to the updates (9-10), our implementation had small regularization terms over the state value estimates \hat{V}_i for each task, in the form of L_2 losses with a coefficient 0.005, to encourage a small amount of transfer of knowledge in value estimates too. We did not tune for this parameter, and believe it is not essential to our results.

Because of the small values of β used, we parameterized β times the soft advantages using the network outputs instead, so that (7-8) read as:

$$\beta \hat{A}_i(a_t|s_t) = f_{\theta_i}(a_t|s_t) - \log \sum_a \hat{\pi}_0^\alpha(a|s_t) \exp(f_{\theta_i}(a|s_t)) \quad (11)$$

$$\hat{\pi}_i(a_t|s_t) = \hat{\pi}_0^\alpha(a_t|s_t) \exp(\beta \hat{A}_i(a_t|s_t)) = \frac{\exp(\alpha h_{\theta_0}(a_t|s_t) + f_{\theta_i}(a_t|s_t))}{\sum_{a'} \exp((\alpha h_{\theta_0}(a'|s_t) + f_{\theta_i}(a'|s_t))} \quad (12)$$

When reporting results for the navigation and laser-tag sets of tasks, we normalized the results by the best performance of a standard A3C agent on a task by task basis, to account for different rewards scales across tasks.

C Detailed learning curves

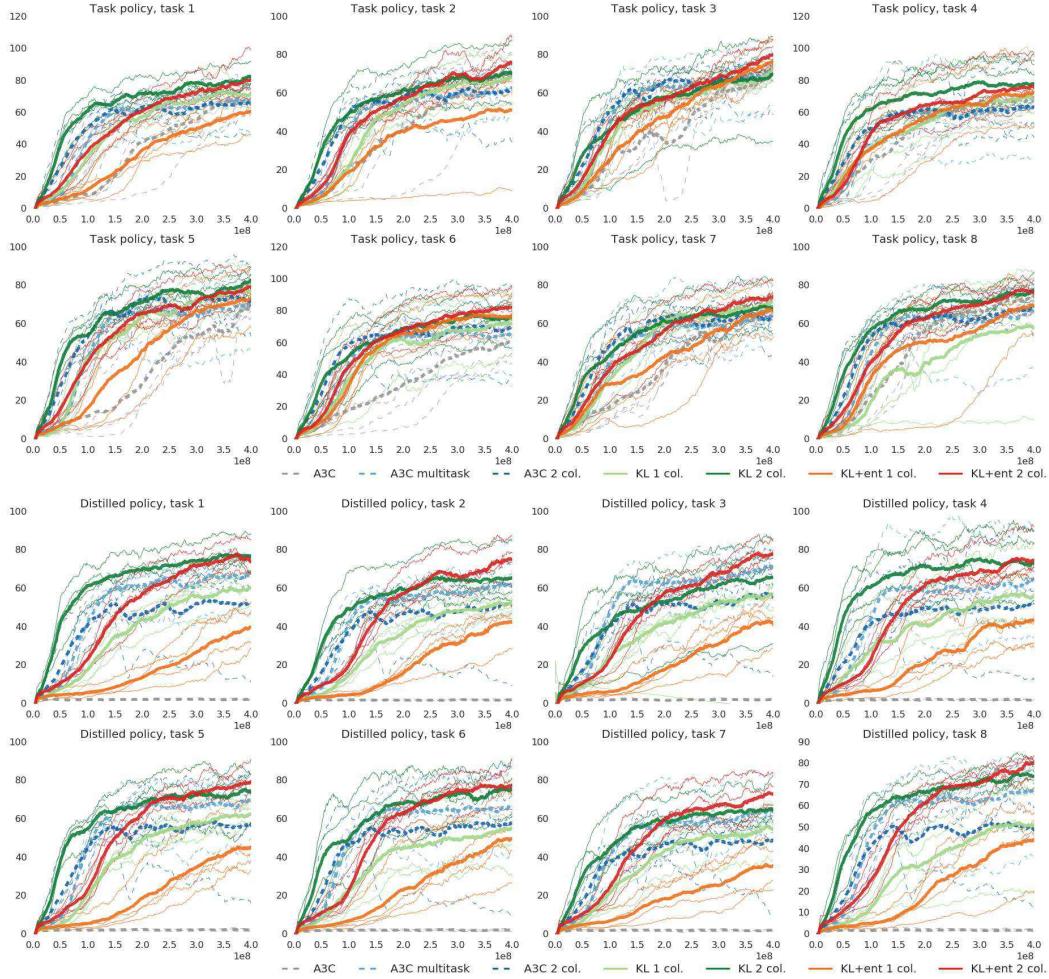


Figure 5: Scores on the 8 different tasks of the navigation suite. Top two rows show the results with the task specific policies, bottom two rows show the results with the distilled policy. For each algorithm, results for the best set of hyperparameters are reported, as obtained by maximizing the averaged (over tasks and runs) areas under curves. For each algorithm, the 4 thin curves correspond to the 4 runs. The average over these runs is shown in bold. The x -axis shows the total number of training environment steps for each task.

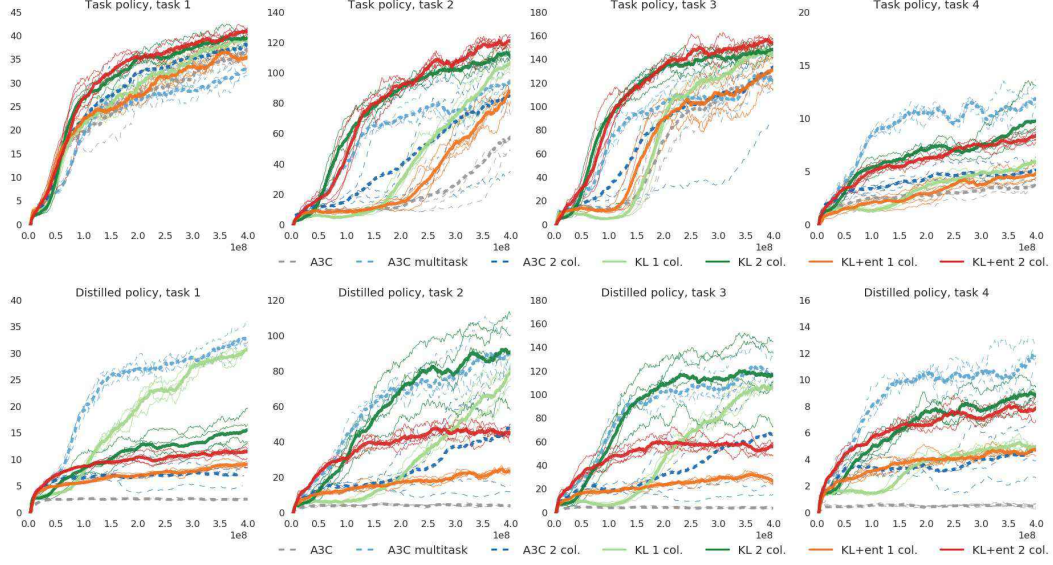


Figure 6: Scores on the 4 different tasks of the navigation suite. Top row shows the results with the task specific policies, bottom row shows the results with the distilled policy. For each algorithm, results for the best set of hyperparameters are reported, as obtained by maximizing the averaged (over tasks and seeds) area under curve. For each algorithm, the 4 curves correspond to the 4 different seeds. The average over these seeds is shown in bold. The x -axis shows the total number of training environment steps for the corresponding task.

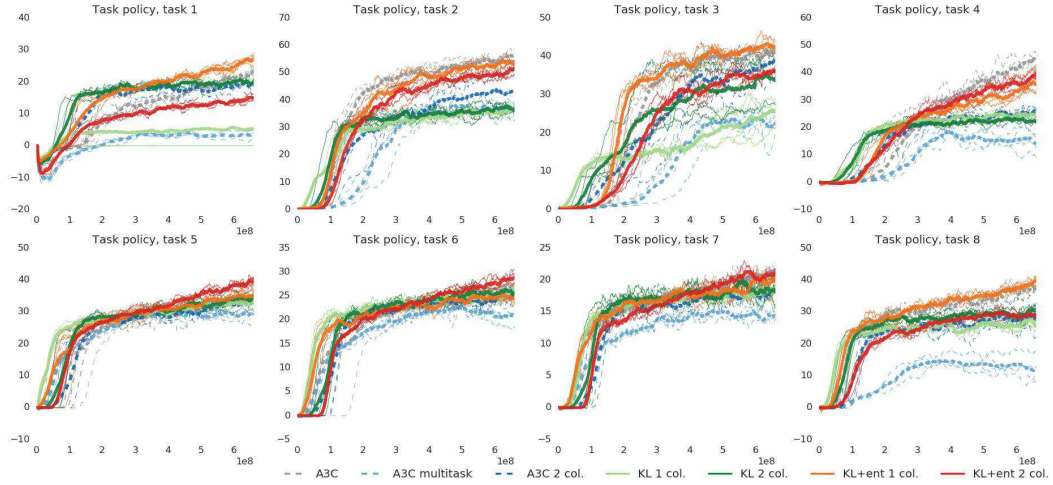


Figure 7: Scores on the 8 different tasks of the laser-tag suite. Only results with the task policies were computed for this set of tasks. For each algorithm, results for the best set of hyperparameters are reported, as obtained by maximizing the averaged (over tasks and seeds) area under curve. For each algorithm, the 4 curves correspond to the 4 different seeds. The average over these seeds is shown in bold. The x -axis shows the total number of training environment steps for the corresponding task.